

# Dynamics of the Concerted Triple Proton Transfer in Cyclic Water Trimer Using the Multiconfiguration Molecular Mechanics Algorithm<sup>†</sup>

Yangsoo Kim and Yongho Kim\*

Department of Chemistry, Kyung Hee University, Yong-In City, Kyunggi-Do, 449-701, Korea

Received: June 7, 2005; In Final Form: September 10, 2005

Cyclic water clusters are important molecular species to understand the nature of hydrogen bonded networks. Theoretical studies for the dynamics of triple proton transfer in the cyclic water trimer were performed. The potential energy surface (PES) of triple proton transfer is generated by the multiconfiguration molecular mechanics (MCMM) algorithm. We have used the MP2/6-31G(d,p) level for high-level ab initio data (energies, gradients, and Hessians), which are used in the Shepard interpolation. Eight high-level reference points were added step by step, including two points for the critical configurations of the large curvature tunneling paths. The more high-level points are used, the better the potential energy surfaces become. The rate constant and kinetic isotope effect (KIE) for the triple proton transfer at 300 K, which have been calculated by the canonical variational transition-state theory with microcanonical optimized multidimensional semiclassical tunneling approximation, are  $1.6 \times 10^{-3} \text{ s}^{-1}$  and 230, respectively. Tunneling is very important not only for the triple proton transfer but also for the triple deuterium transfer. The MCMM results show good agreement with those from the direct ab initio dynamics calculations.

## 1. Introduction

Proton transfer over a long distance is a key step in many biological reactions.<sup>1,2</sup> In most of the long-range proton transfers, water plays an important role in the transfer of protons. The properties (structures, binding energies, thermodynamic quantities, spectra, electronic properties) of small water clusters have been the focus of a large number of experimental<sup>3–21</sup> and theoretical<sup>13,22–46</sup> investigations, due to their importance in understanding solvent effects in biological and chemical systems. Properties of neutral, cyclic water clusters  $(\text{H}_2\text{O})_n$  are important for the understanding of the condensation process and the nature of hydrogen bonded networks.<sup>1,2,47,48</sup> The water trimer has been studied both theoretically and experimentally, and the global minimum was found to be a chiral ring structure of  $C_1$  symmetry with nonlinear hydrogen bonds between the oxygens and three exocyclic O–H bonds, one of which is oriented opposite two others with respect to the plane of the ring.<sup>38</sup> Each oxygen acts as hydrogen donor and acceptor at the same time. The transition state of the concerted triple proton transfer has  $C_s$  symmetry, and the transferring protons are exactly in the middle of the shortened O–O distances.<sup>42</sup>

Puliano and Saykally<sup>12</sup> have reported possible tunneling motions in  $(\text{H}_2\text{O})_3$  via three pathways: flipping of a single external hydrogen from one side of the O–O–O plane to the other, internal  $C_2$  rotation of a single water that it exchanges its external and hydrogen-bonded protons, and a concerted motion that reverses the sense of the hydrogen bonding from either clockwise to counterclockwise or vice versa. Wales<sup>49</sup> has reported rearrangement mechanism, reaction pathways, and the tunneling splittings of the water trimer. However, concerted proton transfer such as that in the clockwise and counterclockwise tunneling motion suggested by Puliano and Saykally<sup>12</sup> has

not been investigated in more detail. Previously discussed motions involve mostly rotational motion of single water molecules,<sup>43,44,49</sup> in which no intermolecular hydrogen transfer (i.e., chemical reaction) occurs. Liedl et al. have studied concerted proton transfer in a cyclic water cluster using variational transition state theory with interpolated correction including a semiclassical tunneling approximation, and they found that tunneling is significant in this reaction.<sup>42,45</sup>

More recently, another efficient algorithm, called multiconfiguration molecular mechanics (MCMM), has been introduced to generate multidimensional potential energy surface.<sup>50–52</sup> This algorithm may be thought of as a dual-level scheme that uses molecular mechanics potential functions as the lower level and electronic structure theory as the higher level. This algorithm can be applied well to the proton-transfer reactions in hydrogen bonded systems since these reactions can be expressed well by a double-well potential function. The potential energy surface of triple proton transfer is generated by the MCMM algorithm in this study. Rate constants and kinetic isotope effects (KIEs) have been calculated by the canonical variational transition-state theory, and these results are compared with those from the direct ab initio dynamics calculations.

## 2. Computational Details

Details of the standard MCMM algorithm can be obtained from the original paper<sup>50</sup> and will not be repeated here. For a geometry  $q$  far from the minima, the energy can be expressed in terms of the two diabatic configurations by solving the secular equation

$$\begin{vmatrix} V_{11} - V & V_{12} \\ V_{12} & V_{22} - V \end{vmatrix} = 0 \quad (1)$$

where the term  $V_{12}(q)$  is called the resonance energy function or resonance integral, and  $V$  denotes the lowest-energy eigen-

\* Corresponding author. Fax: +82-31-203-5774. E-mail: yhkim@khu.ac.kr.

<sup>†</sup> Part of the special issue "Donald G. Truhlar Festschrift".

value of  $V$ . This eigenvalue is given by

$$V(q) = \frac{1}{2} \{ (V_{11}(q) + V_{22}(q)) - [(V_{11}(q) - V_{22}(q))^2 + 4V_{12}(q)^2]^{1/2} \}, \quad (2)$$

The molecular mechanics potentials  $V_{11}(q)$  and  $V_{22}(q)$  are readily available, inexpensive to calculate, and easy to differentiate analytically. The resonance integral  $V_{12}(q)$  and its derivatives are the key features of the MCMM algorithm, and they are obtained using Shepard interpolation.<sup>53,54</sup> The interpolation is based on data at a set of  $M$  points called Shepard points  $q^{(k)}$ , with  $k = 1, 2, \dots, M$ , at which the energies  $V^{(k)}$ , gradients  $g^{(k)}$ , and Hessian matrices  $f^{(k)}$  are available. For a given Shepard point  $q^{(k)}$ ,  $V(q;k)$  is expanded in a Taylor series around  $q^{(k)}$ . After expanding  $V_{11}(q;k)$  and  $V_{22}(q;k)$  using molecular mechanics potential functions, a quadratic expansion of  $V_{12}(q;k)$  around point  $q^{(k)}$  is obtained using eq 2; this was given as eq 13 in ref 50. This quadratic expansion is carried out in internal coordinates to avoid any ambiguity of the orientation of the system in space. Once the quadratic expansion of  $V_{12}(q;k)$  is completed for all the Shepard points,  $V_{12}$  at a desired geometry  $q$  (in internal coordinates) can be evaluated by means of Shepard interpolation as a linear combination of the quadratic expansions around these Shepard points:

$$V_{12}^S(q) = \sum_{k=1}^M W_k(q) V_{12}(q;k), \quad (3)$$

where  $W_k(q)$  is the normalized weight, and the quadratic part is

$$[V_{12}(q;k)]^2 = D^{(k)} \left[ 1 + b^{(k)T}(q - q^{(k)}) + \frac{1}{2}(q - q^{(k)})^T C^{(k)}(q - q^{(k)}) \right] \quad (4)$$

A Shepard interpolation in the MCMM algorithm requires at least three points, which are the minima of the reactant- and product-valley wells and the saddle point. These first three points are all stationary points, and they are the first three Shepard points ( $k = 1, 2$ , and 3) employed in all cases. An MCMM calculation based on these three points without any supplementary points is denoted as MCMM-0. Then  $N_s$  supplementary points can be added successively into the Shepard interpolation, and the corresponding MCMM computation (based overall on  $M = N_s + 3$  points) is labeled MCMM- $N_s$ . In the MCMM interpolation scheme, the reactant- and product-valley wells are completely described at the molecular mechanics level, whereas the other Shepard points (the saddle point and supplementary points) are treated at the higher level of theory, i.e., high-level electronic structure calculations. Therefore, to generate the MCMM potential energy surface, one needs higher-level electronic structure data (energy, gradient, and Hessian) at  $N_s + 1$  points. To perform variational transition state theory computations, additional electronic structure information is required for the reactants, and to calculate the equilibrium constant or reverse rates, such information is required for products too.

The MCMM dynamics calculations were carried out using the MC-TINKERATE<sup>55</sup> program that interfaces the POLYRATE<sup>56</sup> and MC-TINKER<sup>57</sup> programs. As a reference, the direct ab initio dynamics calculations were carried out using GAUSSRATE,<sup>58</sup> which is an interface of POLYRATE<sup>56</sup> with GAUSSIAN.<sup>59</sup> The MM3 force field parameters are used for the molecular mechanics. Because the original parameters of

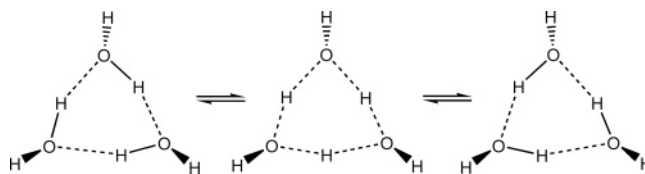


Figure 1. Triple proton transfer in the cyclic water trimer.

the force field cannot reproduce the geometries from the quantum mechanics calculations, we need to modify the existing molecular mechanics parameters or add the new parameters for the undefined atom types. The high level data (structure, energy, and Hessian) for the Shepard interpolation were obtained at the MP2/6-31G(d,p) level.

Rate constants were calculated by canonical variational transition-state-theory (CVT) with semiclassical multidimensional tunneling calculations. Transmission coefficients,  $\kappa$ , were calculated by the small-curvature tunneling (SCT) approximation,<sup>60,61</sup> the large-curvature tunneling (LCT) approximation,<sup>60,62–64</sup> and the microcanonical optimized multidimensional tunneling ( $\mu$ OMT) approximation,<sup>64,65</sup> which are denoted  $\kappa^{\text{SCT}}$ ,  $\kappa^{\text{LCT}}$ , and  $\kappa^{\mu\text{OMT}}$ , respectively.

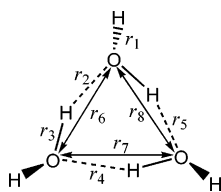
### 3. Results and Discussion

The triple proton transfer in cyclic water trimer occurs in the concerted mechanism as shown in Figure 1. Geometries for water trimer (WT) and the transition state (TS) were optimized at various levels of theory such as MP2/6-31G(d,p), MP2/TZ2P, MP2/cc-pVTZ, and B3LYP/cc-pVTZ. The multicoefficient corrected quantum mechanical methods (MCCM)<sup>66–68</sup> were also used. Table 1 shows the geometrical parameters for water trimer and the transition state at various levels of theory. Cyclic water trimer is more stable than open-chained water trimer.<sup>12,36</sup> In the optimized geometry of water trimer at the MP2 level, the hydrogen bond lengths using the TZ2P basis set are slightly longer than those with the 6-31G(d,p) and cc-pVTZ basis sets, but quite similar to those from the MCCM-UT-MP4SDQ and MCCM-UT-CCSD methods. Loerting et al.<sup>45</sup> have reported that the distances between oxygens in the water trimer were 2.791–2.798 Å at the MP2/6-311++G(3pd,3df) level, which agree well with the MP2/TZ2P and MCCM results.

The transition state has  $C_s$  symmetry, in which  $H_7$  is centered exactly in the middle of two oxygens,  $O_2$  and  $O_3$ . The bond distances between the bridging hydrogen and oxygen are in the range from 1.196 to 1.223 Å depending on the computational methods. The bridging OH bonds in the optimized TS at the MCCM-UT-MP4SDQ and MCCM-UT-CCSD levels are slightly shorter than those at the MP2/TZ2P level, and they agree very well with the MP2/cc-pVTZ results. The O–O distances become shorter by about 0.4 Å as the reaction goes from reactant to TS.

The barrier heights and imaginary frequencies are listed in Table 2. The potential energy barriers depend not only on the computational level but also on the size of basis sets. The HF level predicts a higher barrier than the MCCM methods, whereas the MP2 and B3LYP predict lower barriers except for the MP2/TZ2P. The frequencies of reactant and transition state have been calculated at the MP2 and B3LYP levels. The symmetric O–O stretching frequencies for the reactant and TS are listed in Table 3, and these motions are illustrated in Figure 2. This frequency is increased on going from the reactant toward the transition state, which is attributed to the reduced O–O bond distance.

A full ab initio calculation of reaction dynamics is time-consuming. Generation of an energy point on the minimum

**TABLE 1: Geometric Parameters for Water Trimer and the Transition State<sup>a</sup>**


	$r_1$	$r_2$	$r_3$	$r_4$	$r_5$	$r_6$	$r_7$	$r_8$
Complex								
MCCM-UT-MP4SDQ	0.958	1.900	0.970	1.916	1.897	2.793	2.796	2.788
MCCM-UT-CCSD	0.959	1.900	0.971	1.918	1.897	2.795	2.799	2.791
HF/6-31G(d,p)	0.944	1.997	0.952	2.024	2.000	2.871	2.884	2.869
B3LYP/cc-pVTZ	0.961	1.878	0.977	1.894	1.871	2.784	2.790	2.777
MP2/6-31G(d,p)	0.962	1.882	0.976	1.899	1.879	2.788	2.802	2.785
MP2/TZ2P	0.958	1.897	0.972	1.919	1.896	2.795	2.802	2.793
MP2/cc-pVTZ	0.959	1.873	0.974	1.890	1.871	2.778	2.784	2.775
Transition State								
MCCM-UT-MP4SDQ	0.959	1.211	1.212	1.213	1.212	2.365	2.363	2.365
MCCM-UT-CCSD	0.959	1.212	1.212	1.214	1.212	2.367	2.365	2.367
HF/6-31G(d,p)	0.944	1.196	1.200	1.199	1.200	2.335	2.333	2.335
B3LYP/cc-pVTZ	0.961	1.220	1.222	1.223	1.222	2.384	2.383	2.384
MP2/6-31G(d,p)	0.964	1.214	1.215	1.216	1.215	2.372	2.371	2.372
MP2/TZ2P	0.960	1.217	1.218	1.219	1.218	2.377	2.375	2.377
MP2/cc-pVTZ	0.961	1.213	1.215	1.215	1.215	2.373	2.371	2.373

<sup>a</sup> Distances are in Å.**TABLE 2: Barrier Heights and Imaginary Frequencies for the TS of the Triple Proton Transfer in the Cyclic Water Trimer at Various Levels of Theory**

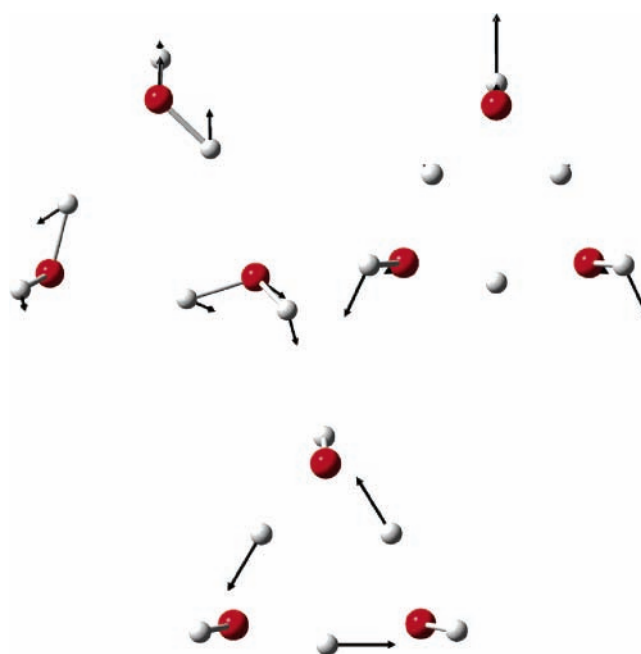
computational levels	$E^\ddagger$ <sup>a</sup>	$\nu^\ddagger$ <sup>b</sup>
MCCM-UT-MP4SDQ	28.77	1907 <i>i</i>
MCCM-UT-CCSD	28.67	1908 <i>i</i>
HF/6-31G(d,p)	46.44	2308 <i>i</i>
MP2/6-31G(d,p)	26.90	1861 <i>i</i>
MP2/TZ2P	28.77	1901 <i>i</i>
MP2/cc-pVTZ	25.62	1819 <i>i</i>
B3LYP/cc-pVTZ <sup>c</sup>	25.32	1807 <i>i</i>
MP2/6-311++G(3pd,3df) <sup>d</sup>	26.99	1833 <i>i</i>
B3LYP/6-31+G(d) <sup>d</sup>	26.99	1842 <i>i</i>
B3LYP/6-311++G(3pd,3df) <sup>e</sup>	26.30	1815 <i>i</i>

<sup>a</sup> Barrier heights are in kcal/mol. <sup>b</sup> Imaginary frequencies are in  $\text{cm}^{-1}$ .  
<sup>c</sup> Reference 46. <sup>d</sup> Reference 45. <sup>e</sup> Reference 42.**TABLE 3: Symmetric O–O Stretching Frequencies of the Minimum Energy Structure and the Transition State<sup>a</sup>**

	minimum energy structure	transition state
HF/6-31G(d,p)	214	794
MP2/6-31G(d,p)	241	753
MP2/TZ2P	223	738
MP2/cc-pVTZ	228	746
B3LYP/cc-pVTZ <sup>b</sup>	231	731
MP2/6-311++G(3pd,3df) <sup>c</sup>	217	741
B3LYP/6-311++G(3pd,3df) <sup>d</sup>	216	729

<sup>a</sup> Frequencies are in  $\text{cm}^{-1}$ . <sup>b</sup> Reference 46. <sup>c</sup> Reference 45. <sup>d</sup> Reference 42.

energy path (MEP) may take hours or more, and obtaining a converged reaction rate constant requires a large number of energies, Hessians, and gradients calculations. We have used the MCM algorithm<sup>50</sup> to calculate the dynamics of triple proton transfer with minimum number of high level ab initio calculations. We have chosen the MP2/6-31G(d,p) method after considering the computational cost and accuracy. The barrier height at this level agrees very well with that using the MP2/6-311++G(3pd,3df) method by Loerting et al.,<sup>45</sup> although it is slightly smaller than the MCCM values.

**Figure 2.** Symmetric O–O stretching modes of  $(\text{H}_2\text{O})_3$  minimum energy structure (top left) and transition state (top right) and proton-transfer mode corresponding to the imaginary frequencies of transition state (bottom).

In the MCM methods, the geometries of the reactant and product for the triple proton transfer are used as the configurations of the potential wells (minimum points on the potential energy surface). They are calculated with the molecular mechanics using the MM3 force field. Figure 3 shows the structure obtained with the standard MM3 force field parameters, which is quite different from the quantum mechanical structure. We have modified the standard MM3 parameters and added missing parameters to reproduce the quantum mechanical structure. The structure from the modified MM3 parameters is also shown. It is important to have reasonably good force field parameters for successful MCM calculations. The convergence

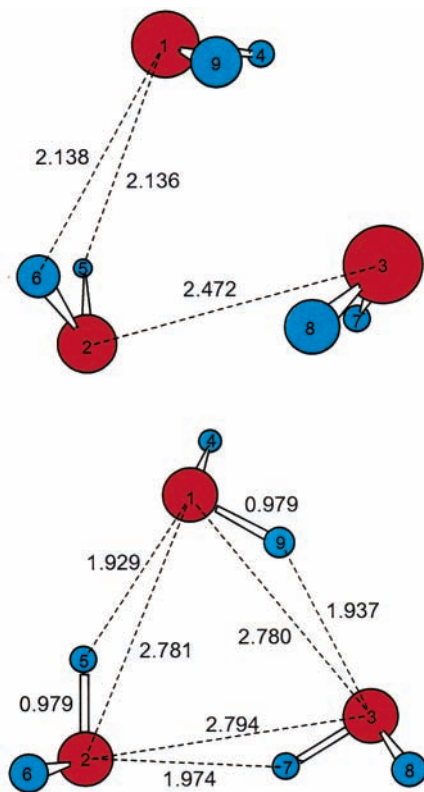


**Figure 3.** Geometric parameters of water trimer optimized with the standard (top) and the modified (bottom) MM3 force field parameters. Distances are in Å.

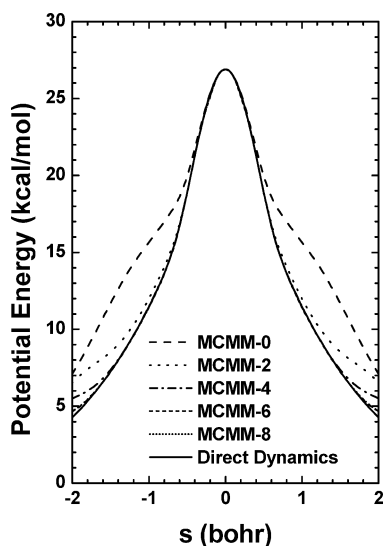


**Figure 4.** Potential energies along the reaction coordinate of the triple proton transfer in the cyclic water trimer.

of the computed properties, such as rate constants and transmission coefficients, depends on the quality of the force field parameters. The modified and new parameters are listed in Supporting Information.

The Born–Oppenheimer potential energy curves and the vibrationally adiabatic ground-state potential energy curves along the MEP obtained from the MCMM calculations are represented in Figures 4 and 5, respectively. The potential and adiabatic energy curves calculated from the direct ab initio dynamics are also displayed as solid lines. Other lines except a solid line are the curves obtained from the MCMM algorithm. To obtain the final potential energy curve from the MCMM

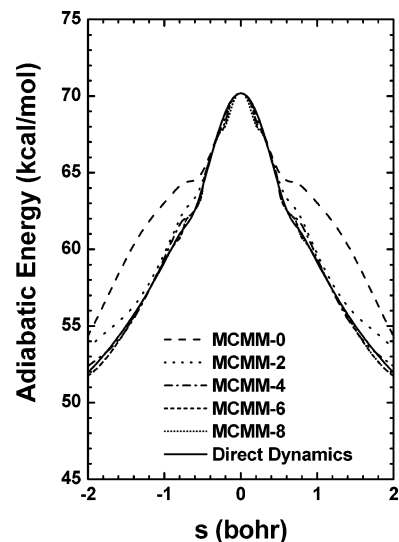


**Figure 5.** Vibrationally adiabatic ground-state potential energies along the reaction coordinate of the triple proton transfer in the cyclic water trimer.

algorithm, we have used nine high-level quantum mechanical points including the TS. In the MCMM-0 calculation, three points (two wells and TS) were used for the Shepard interpolation and the resulting MCMM-0 curves are represented as a dashed line in Figures 4 and 5. The MCMM-0 curve is the outcome of interpolating three curves originated from the reactant, product, and TS. Two curves for the reactant and product are based on the MM3 force field and one for the TS is based on the high-level quantum mechanics. In the previous study,<sup>50,51</sup> the first supplementary point is taken to be along the MEP of the MCMM-0 run, below the saddle point in energy by one-fourth of the barrier height. However this is rather arbitrary and does not necessarily give the best result. In the potential and adiabatic energy curves, there are regions where the curvature begins to change. Below this region the MM3 force field seems to affect more to the curves and above the high-level quantum mechanics seems to have more influence to the potential surface. So we chose the first additional points at  $s = -0.40 a_0$  and  $s = +0.40 a_0$ , where the potential and adiabatic energy curves begin to swell out, and calculated the electronic structures, gradients, and Hessian for those points. These points happen to be about one-fourth of the way below the top of the barrier in energy. We have calculated a new MCMM dynamics including these two additional reference points, which is called MCMM-2. The MCMM-2 potential and adiabatic energy curves are represented as dotted lines in Figures 4 and 5, respectively. The convex region in the MCMM-0 potential curve at  $s < -0.40 a_0$  and  $s > +0.40 a_0$  is disappeared in the MCMM-2 curve; however, there still exists some undulation in the adiabatic energy curve. The MCMM-4 calculation uses five high-level points with two additional points at  $s = -0.6 a_0$  and  $s = +0.6 a_0$ . These additional points were selected because the MCMM-2 adiabatic energy curve swelled out slightly below these points. The undulation in the adiabatic energy curve became smaller, but did not disappear completely. So we selected two additional points again at  $s = -1.0 a_0$  and  $s = +1.0 a_0$ , which jump over the convex regions. The MCMM-6 potential and adiabatic energy curves with seven high-level points are shown as short-dashed lines in Figures 4 and 5, respectively. The MCMM-6 potential energy curve agrees very well with that from the direct ab initio dynamics calculation along the entire reaction path between  $s = -2.0 a_0$  and  $s =$

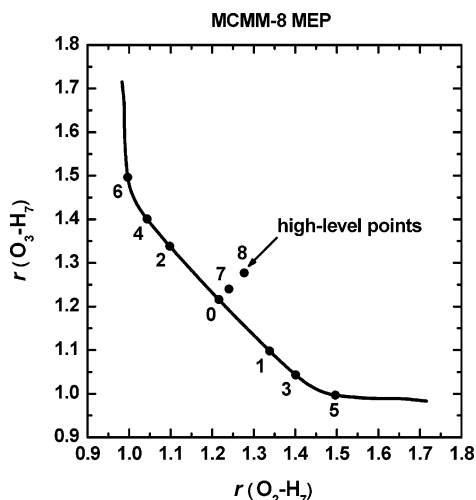


**Figure 6.** Two-dimensional representation of the MEP and the location of Shepard points for the MCMM-8 calculation.

+2.0  $a_0$ . The adiabatic energy curve still has slight undulation, but it matches quite well with that from the direct ab initio dynamics.

Since the proton exchange has a heavy–light–heavy mass combination, the large-curvature tunneling (LCT) approximation should be considered. To obtain better LCT coefficients, we have added extra reference points on the representative LCT path for the temperature of interest. We have added two electronic structures for the critical configurations in the middle of the tunneling path where the LCT is maxima at 300 and 250 K. These calculations are called MCMM-7 and MCMM-8, respectively. The MCMM-7 and MCMM-8 calculations did not improve the shape of the MCMM-6 curves any more. The MCMM-8 potential and adiabatic energy curves are represented as short-dotted lines in Figures 4 and 5, respectively. The final MCMM dynamics calculation uses nine high-level points with seven points on the MEP and two on the LCT path. The MCMM potential energy surfaces became better and closer to the direct ab initio dynamics surface as the number of high-level points is increased. Two-dimensional representations of the MEP from the MCMM-8 calculation and the locations of the high-level quantum mechanical points are plotted in Figure 6. The  $X$  and  $Y$  axes are the distances of the making and the breaking bonds,

$O_2-H_7$  and  $O_3-H_7$ , respectively. Point 0 is located on the saddle point, points 1, 3, and 5 are chosen on the reactant side, points 2, 4, and 6 are chosen on the product side, and points 7 and 8 are located on the critical configuration of the LCT path.

Figure 7 shows the  $O-H$  bond lengths and the distances between two  $O$  atoms ( $O_2$  and  $O_3$ ) along the MEP of the MCMM-8 and direct dynamics potential energy surfaces. The  $O_3-H_7$  bond length is rarely changed at  $s < -0.76 a_0$ . But the  $O_2-H_7$  hydrogen bond length is decreased from 1.638 ( $s = -2.00 a_0$ ) to 1.445 Å ( $s = -0.76 a_0$ ) and the  $O_2-O_3$  distance is decreased from 2.532 to 2.386 Å as well. The  $O_3-H_7$  bond length is increased rapidly from 1.013 to 1.445 Å between  $s = -0.75 a_0$  and  $s = +0.75 a_0$ , while the  $O_2-O_3$  distance is rarely changed. These results suggest that in the early stage of the reaction the  $O$  atoms of the trimer come closer with almost no change in the  $O-H$  bond length, and when the  $O$  atoms reach a certain distance (about 2.39 Å), the protons jump quickly without changing the  $O-O$  distance much. This behavior is due to the separation of heavy atom motion from the light atom motion that has been observed many proton-transfer reactions.<sup>69–71</sup> The variation of the bond lengths along the MEP is almost identical for both the MCMM-8 and direct ab initio dynamics calculations. Figure 8 shows the generalized frequencies along the reaction coordinates for the triple proton transfer. The vibrational modes from the MCMM-8 potential surface show good agreement with those from the direct ab initio dynamics although there exist a small fluctuation. This fluctuation in frequencies causes the undulation in the adiabatic energy curves as shown in Figure 5.

Transmission coefficients for the triple proton and deuterium transfer are listed in Tables 4–6. In all the MCMM runs, the SCT transmission coefficients are larger than the LCT ones at 300 K for both proton and deuterium transfer. This implies that the reaction path curvature near the saddle point is rather small. The more high-level points on the MEP are used, the larger transmission coefficients become. The MCMM-6 calculation slightly overestimates the LCT values of triple proton transfer below 300 K and underestimates above comparing with the direct dynamics results. The MCMM-8 calculation with two additional high-level points at the critical configuration of the LCT path gives smaller LCT values below 300 K, and larger values above, which makes overall LCT values closer to the

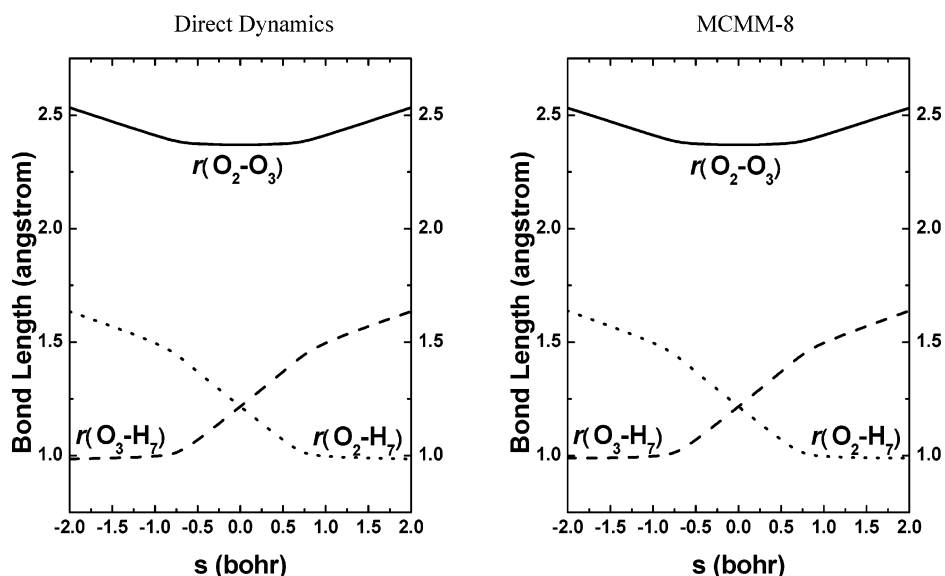


**Figure 7.** Bond distances along the minimum energy path.

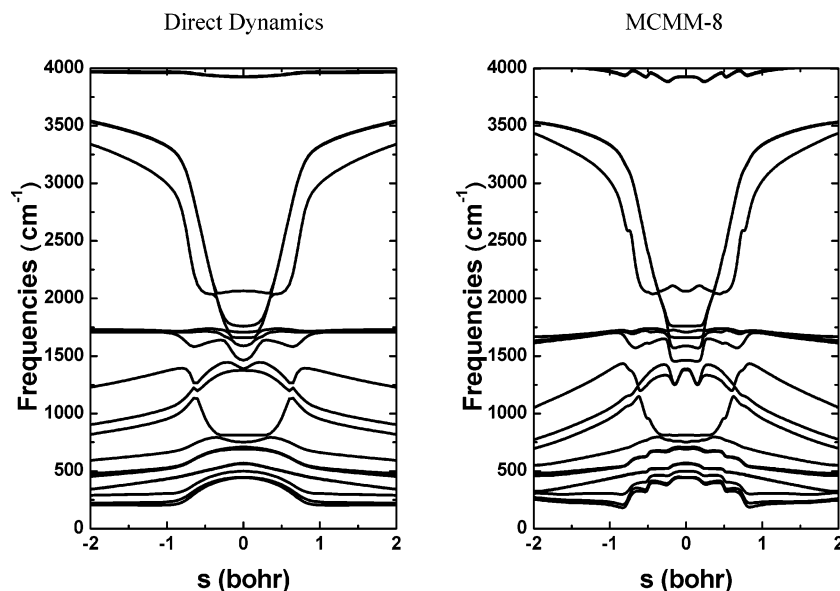


Figure 8. Generalized frequencies for the triple proton transfer as functions of reaction coordinate.

TABLE 4: Small-Curvature Tunneling Coefficients at Various Temperatures<sup>a</sup>

T (K)	MCOMM-0	MCOMM-2	MCOMM-4	MCOMM-6	MCOMM-8	direct dynamics
250	1.97E+02 (3.00E+01)	1.50E+03 (5.08E+01)	2.05E+03 (5.95E+01)	2.93E+03 (7.03E+01)	2.93E+03 (7.30E+01)	4.62E+03 (1.00E+02)
300	3.51E+01 (7.90E+00)	8.57E+01 (9.56E+00)	1.07E+02 (1.08E+01)	1.30E+02 (1.21E+01)	1.35E+02 (1.33E+01)	1.65E+02 (1.07E+01)
400	6.45E+00 (2.73E+00)	7.93E+00 (2.99E+00)	8.99E+00 (3.25E+00)	9.81E+00 (3.51E+00)	1.09E+01 (3.86E+00)	2.54E+01 (4.35E+00)
500	3.11E+00 (1.83E+00)	3.37E+00 (1.94E+00)	3.67E+00 (2.05E+00)	3.91E+00 (2.16E+00)	4.35E+00 (2.33E+00)	8.93E+00 (2.79E+00)

<sup>a</sup> Numbers in parentheses are for triple deuterium transfer.

TABLE 5: Large-Curvature Tunneling Coefficients at Various Temperatures<sup>a</sup>

T (K)	MCOMM-0	MCOMM-2	MCOMM-4	MCOMM-6	MCOMM-8	direct dynamics
250	1.13E+02 (1.91E+01)	7.34E+02 (3.52E+01)	2.15E+03 (4.73E+01)	4.95E+03 (5.73E+01)	3.27E+03 (6.09E+01)	2.20E+03 (3.48E+01)
300	2.33E+01 (6.30E+00)	4.62E+01 (8.32E+00)	6.90E+01 (9.55E+00)	9.70E+01 (1.06E+01)	9.48E+01 (1.20E+01)	6.45E+01 (6.74E+00)
400	5.11E+00 (2.55E+00)	6.39E+00 (2.84E+00)	7.32E+00 (3.07E+00)	8.21E+00 (3.34E+00)	9.33E+00 (3.75E+00)	1.28E+01 (3.49E+00)
500	2.70E+00 (1.78E+00)	3.07E+00 (1.88E+00)	3.35E+00 (1.98E+00)	3.65E+00 (2.11E+00)	4.12E+00 (2.30E+00)	5.81E+00 (2.46E+00)

<sup>a</sup> Numbers in parentheses are for triple deuterium transfer.

direct ab initio dynamics results. The SCT transmission coefficients become slightly larger in general.

In the direct dynamics, the SCT transmission coefficients are larger than the LCT ones, which is consistent with the MCOMM calculations. This result suggests that the reaction path curvature is small. Liedl and co-workers have performed dual-level direct ab initio dynamics calculation based on the B3LYP/6-31+G(d) level for the MEP and the MP2/6-311++G(3pd,3df) level for three higher level points. They have reported that the LCT coefficient is larger than the SCT one, whereas in our direct ab initio calculations the SCT values are larger than the LCT values at 200 K and above. (The values at 200 K are not listed in Tables 4 and 5.) The large curvature ground-state approximation version 3 (LCG3) has been improved to version 4 (LCG4) because it sometimes overestimates the tunneling probability at low energy.<sup>72</sup> This new LCT method tends to give smaller tunneling coefficients than the old method, which might change the relative importance of the LCT vs SCT.

All the MCOMM calculations slightly underestimate the SCT values compared with the direct dynamics calculation. The  $\mu$ OMT transmission coefficient estimates the optimal transmission probability as the larger of the transmission probabilities evaluated by the SCT and LCT approximations at a given energy.<sup>64</sup> The  $\mu$ OMT coefficients at 300 K are 1420 and 134 for triple proton and deuterium transfers, respectively. Not only proton but deuterium tunneling is very significant as well. The  $\kappa_{\text{HHH}}^{\text{LCT}}$  values from the MCOMM-8 calculation are larger than  $\kappa_{\text{HHH}}^{\text{SCT}}$  values at 250 K, but smaller at 300 K and above, which means that the relative importance of the SCT and the LCT tunneling switches at temperature between 250 and 300 K. Figure 9 shows the ground-state transmission probabilities,  $P^{\text{G}}(E)$ , calculated by the SCT and the LCT approximations as a function of  $V_a^{\text{G}}$  at the reaction coordinate turning point. The  $P^{\text{G}}(E)$  values from the SCT approximation are larger than those from the LCT at energies

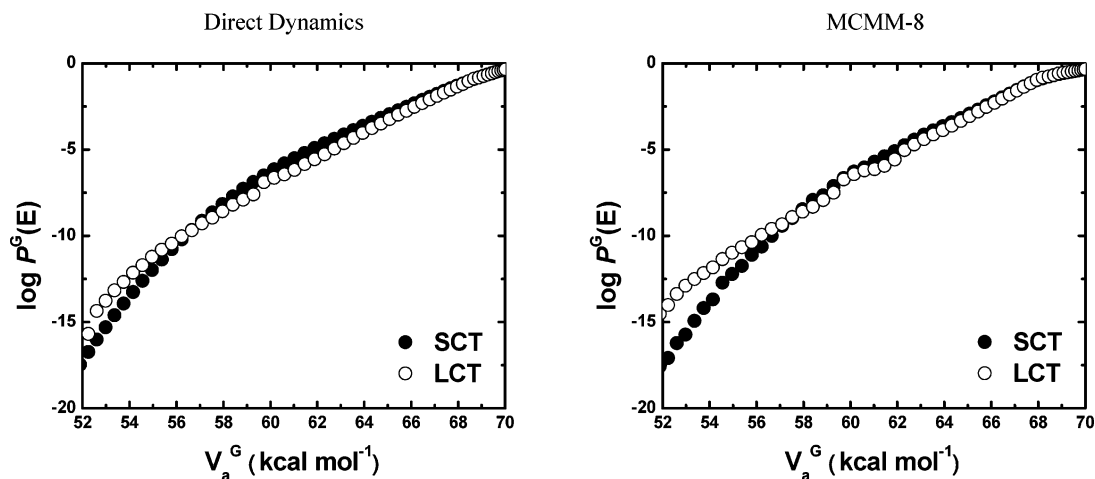


**Figure 9.** Transmission probability for the triple proton transfer as a function of the adiabatic energy at the reaction coordinate turning point. The open and fill circles are for the values from the LCT and SCT approximations, respectively. Note that  $V_a^G$  at the reaction coordinate turning point is the same as the total energy  $E$ .

**TABLE 6: Microcanonical Optimized Multidimensional Tunneling Coefficients at Various Temperatures<sup>a</sup>**

$T$ (K)	MCMM-0	MCMM-2	MCMM-4	MCMM-6	MCMM-8	direct dynamics
250	1.97E+02 (3.01E+01)	1.58E+03 (5.08E+01)	3.13E+03 (6.09E+01)	6.04E+03 (7.49E+01)	4.38E+03 (7.67E+01)	5.10E+03 (1.00E+02)
300	3.51E+01 (7.94E+00)	8.63E+01 (9.56E+00)	1.14E+02 (1.08E+01)	1.45E+02 (1.22E+01)	1.42E+02 (1.34E+01)	1.68E+02 (1.07E+01)
400	6.45E+00 (2.75E+00)	7.94E+00 (2.99E+00)	9.03E+00 (3.25E+00)	9.95E+00 (3.53E+00)	1.10E+01 (3.91E+00)	2.55E+01 (4.37E+00)
500	3.11E+00 (1.84E+00)	3.38E+00 (1.94E+00)	3.69E+00 (2.05E+00)	3.97E+00 (2.17E+00)	4.43E+00 (2.36E+00)	8.95E+00 (2.81E+00)

<sup>a</sup> Numbers in parentheses are for triple deuterium transfer.

**TABLE 7: Rate Constants ( $s^{-1}$ ) for the Triple Proton Transfer in the Cyclic Water Trimer<sup>a</sup>**

$T$ (K)	$k_{\text{HHH}}^{\text{CVT}}$	$k_{\text{HHH}}^{\text{CVT/SCT}}$	$k_{\text{HHH}}^{\text{CVT/LCT}}$	$k_{\text{HHH}}^{\text{CVT}/\mu\text{OMT}}$	direct dynamics
250	7.66E-09 (2.16E-10)	2.25E-05 (1.58E-08)	2.51E-05 (1.32E-08)	3.35E-05 (1.66E-08)	3.88E-05 (2.13E-08)
300	1.13E-05 (5.25E-07)	1.52E-03 (6.98E-06)	1.07E-03 (6.32E-06)	1.61E-03 (7.06E-06)	1.89E-03 (5.55E-06)
400	8.85E-02 (7.71E-03)	9.61E-01 (2.97E-02)	8.25E-01 (2.89E-02)	9.76E-01 (3.01E-02)	7.89E-01 (2.14E-02)
500	1.74E+01 (2.25E+00)	7.56E+01 (5.25E+00)	7.15E+01 (5.19E+00)	7.70E+01 (5.31E+00)	5.78E+01 (4.08E+00)

<sup>a</sup> Numbers in parentheses are for triple deuterium transfer.

above 57.7 kcal/mol and smaller below 57.7 kcal/mol. This means that the reaction path curvature of the potential energy surface may be considered small at energies above 57.7 kcal/mol, but large below 57.7 kcal/mol. At low temperature tunneling occurs mostly where the reaction path curvature is large, which makes the LCT coefficients larger than the SCT ones. This behavior is also observed in the direct ab initio dynamics calculation.

The CVT rate constant is denoted  $k^{\text{CVT}}$ , and the rate constant including tunneling is  $k^{\text{CVT}/G} = \kappa^G k^{\text{CVT}}$ , where  $G = \text{SCT}, \text{LCT},$  or  $\mu\text{OMT}$ . The rate constants for the triple proton (deuterium) transfer from the MCMM-8 calculation are listed in Table 7. The  $k_{\text{HHH}}^{\text{CVT}/\mu\text{OMT}}$  and  $k_{\text{DDD}}^{\text{CVT}/\mu\text{OMT}}$  values from MCMM-8 are slightly larger than those from the direct dynamics in general except for the  $k_{\text{HHH}}^{\text{CVT}/\mu\text{OMT}}$  at 300 K. Figure 10 shows the Arrhenius plot for the rate constants with and without tunneling. The rate constants with the  $\mu\text{OMT}$  approximation from the MCMM-8 calculation agree well with the direct ab initio dynamics results. In the previous dynamics studies, the thermal rate constants with tunneling corrections for triple proton transfer are  $k^{\text{LCT}}(300 \text{ K})^{45} = 3.4 \times 10^{-4} \text{ s}^{-1}$  and  $k(300 \text{ K})^{46} = 3.1 \times 10^4 \text{ s}^{-1}$  from dual-level direct dynamics (DLDD)<sup>73–75</sup>

and instanton theory,<sup>76,77</sup> respectively. Our MCMM-8 rate constants are  $k_{\text{HHH}}^{\text{CVT}/\text{SCT}} = 1.52 \times 10^{-3} \text{ s}^{-1}$ ,  $k_{\text{HHH}}^{\text{CVT}/\text{LCT}} = 1.07 \times 10^{-3} \text{ s}^{-1}$ , and  $k_{\text{HHH}}^{\text{CVT}/\mu\text{OMT}} = 1.61 \times 10^{-3} \text{ s}^{-1}$ , at 300 K. These rate constants are slightly larger than the DLDD values, although the potential barrier used in this study is almost identical to that of the DLDD, which is 27.0 kcal/mol. The  $k^{\text{CVT}}$  value of our direct ab initio dynamics calculation is also slightly larger than the DLDD value ( $4.5 \times 10^{-6} \text{ s}^{-1}$ ). The instanton theory overestimates the rate constant by 7 orders of magnitude, which is probably due to abnormally large tunneling effect.

The calculated kinetic isotope effects (KIEs) at various temperatures are listed in Table 8. The KIEs from the MCMM-8 dynamics calculation show good agreement with those from the direct ab initio dynamics.

The direct ab initio dynamics calculation at the MP2/6-31G(d,p) level including semiempirical tunneling approximation takes about 40 h of CPU time, whereas it takes about 1.3 h for 9 high-level electronic structure calculations for the Shepard interpolation and 7 MCMM calculations on our Pentium-based workstation (P4-2.4 GHz, 1 GB RAM, Redhat Linux 8.0). The MCMM calculation reduces the computational cost by about 30 times.

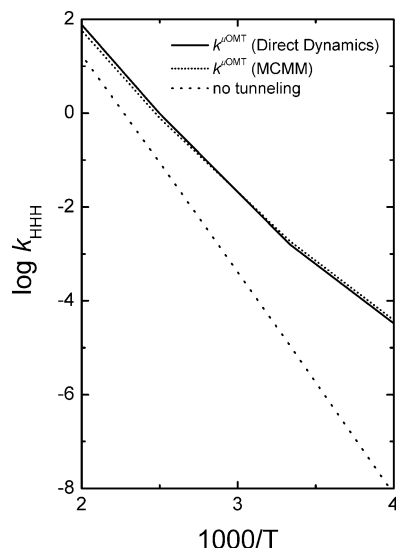


**Figure 10.** Arrhenius plot for the rate constants of the triple proton transfer using the  $\mu$ OMT approximation at various temperatures.

**TABLE 8: Kinetic Isotope Effects**

T (K)	$k_{\text{HHH}}^{\text{CVT}}/k_{\text{DDD}}^{\text{CVT}}$	$k_{\text{HHH}}^{\text{CVT}/\mu\text{OMT}}/k_{\text{DDD}}^{\text{CVT}/\mu\text{OMT}}$	$k_{\text{HHH}}^{\text{CVT}/\mu\text{OMT}}/k_{\text{DDD}}^{\text{CVT}/\mu\text{OMT}}$	direct dynamics
250	35.5	57.0	2023	1818
300	21.5	10.6	228	340
400	11.5	2.8	32.4	36.9
500	7.7	1.9	14.5	14.2

#### 4. Conclusions

This study shows that the potential energy surface (PES) of the concerted triple proton transfer in cyclic water trimer can be generated by the molecular mechanics potential functions with the modified MM3 force field parameters and a limited number of high-level electronic structure calculations. The more high-level quantum mechanical points are used, the better the potential and adiabatic energy surfaces become.

The use of only four high-level points gives a good overall shape of the potential energy curve. Two additional reference points at the critical configuration in the LCT paths improve the LCT coefficients compared with the direct dynamics results. The rate constants and the KIES from the MCMM-8 calculation agree well with our direct dynamics results and previous studies.

**Acknowledgment.** This work is supported by a grant from the Korea Research Foundation (KRF-2002-070-C00048).

**Supporting Information Available:** Table of the modified and added MM3 parameters. This material is available free of charge via the Internet at <http://pubs.acs.org>.

#### References and Notes

- Jeffrey, G. A.; Saenger, W. *Hydrogen Bonding in Biological Structures*; Springer-Verlag: Berlin, 1991.
- Bountis, T.; Ed. *Proton Transfer in Hydrogen-bonded Systems*; Plenum Press: New York, 1992.
- Pimentel, G. C.; Sederholm, C. H. *J. Chem. Phys.* **1956**, *24*, 639.
- Fredin, L.; Nelander, B.; Ribbegard, G. *J. Chem. Phys.* **1977**, *66*, 4065.
- Engdahl, A.; Nelander, B. *J. Chem. Phys.* **1987**, *86*, 1819.
- Engdahl, A.; Nelander, B. *J. Chem. Phys.* **1987**, *86*, 4831.
- Page, R. H.; Frey, J. G.; Shen, Y.-P.; Lee, Y. T. *Chem. Phys. Lett.* **1984**, *106*, 373.
- Coker, D. F.; Miller, R. E.; Watts, R. O. *J. Chem. Phys.* **1985**, *82*, 3554.
- Dyke, T. R.; Muentner, J. S. *J. Chem. Phys.* **1972**, *57*, 5011.
- Curtiss, L. A.; Frurips, D. L.; Blander, M. *Chem. Phys. Lett.* **1978**, *54*, 575.
- Curtiss, L. A.; Frurips, D. L.; Blander, M. *J. Chem. Phys.* **1979**, *71*, 2703.
- Pugliano, N.; Saykally, R. J. *Science* **1992**, *257*, 1937.
- Cruzan, J. D.; Braly, L. B.; Liu, K.; Brown, M. G.; Cruzan, J. D.; Saykally, R. J. *Science* **1996**, *271*, 62.
- Brown, M. G.; Viant, M. R.; McLanghlin, R. P.; Keoshian, C. J.; Cruzan, J. D.; Saykally, R. J. *J. Chem. Phys.* **1999**, *111*, 7789.
- Liu, K.; Brown, M. G.; Carter, C.; Saykally, R. J.; Gregory, J. K.; Clary, D. C. *Nature (London)* **1996**, *381*, 501.
- Huisken, F.; Kaloudis, M.; Kulcke, A. *J. Chem. Phys.* **1996**, *104*, 17.
- Buck, U.; Ettischer, I.; Melzer, M.; Buch, V.; Sadlej, J. *Phys. Rev. Lett.* **1998**, *80*, 2578.
- Brudermann, J.; Melzer, M.; Buck, U.; Kazimirski, J. K.; Sadlej, J.; Buch, V. *J. Chem. Phys.* **1999**, *110*, 10649.
- Nauta, K.; Miller, R. E. *Science* **2000**, *287*, 293.
- Goss, L. M.; Sharpe, W. W.; Blake, T. A.; Vaida, V.; Braut, J. W. *J. Phys. Chem.* **1999**, *103*, 8620.
- Bjorneholm, O.; Federmann, F.; Kakar, S.; Moller, T. *J. Chem. Phys.* **1999**, *111*, 546.
- Morokuma, K.; Pederson, L. *J. Chem. Phys.* **1968**, *48*, 3275.
- Morokuma, K.; Winick, J. R. *J. Chem. Phys.* **1970**, *52*, 1301.
- Del Bene, J. E.; Pople, J. A. *J. Chem. Phys.* **1969**, *4*, 426.
- Hankins, D.; Moskowitz, J. W.; Stillinger, F. H. *J. Chem. Phys.* **1970**, *53*, 4544.
- Kim, K. S.; Dupuis, M.; Lie, G. C.; Clementi, E. *Chem. Phys. Lett.* **1986**, *131*, 451.
- Lee, H. M.; Suh, S. B.; Lee, J. Y.; Tarakeshwar, P.; Kim, K. S. *J. Chem. Phys.* **2000**, *112*, 9759.
- Lee, H. M.; Suh, S. B.; Kim, K. S. *J. Chem. Phys.* **2001**, *114*, 10749.
- Lee, H. M.; Suh, S. B.; Kim, K. S. *J. Chem. Phys.* **2001**, *115*, 7331.
- Maheshwary, S.; Patel, N.; Sathyamurthy, N.; Kulkarni, A. D.; Gadre, S. R. *J. Phys. Chem. A* **2001**, *105*, 10525.
- Pugliano, N.; Cruzan, J. D.; Loeser, J. G.; Saykally, R. J. *J. Chem. Phys.* **1993**, *98*, 6600.
- Pribble, R. N.; Zwier, T. S. *Science* **1994**, *265*, 75.
- Kim, J.; Lee, J. Y.; Mhin, B. J.; Kim, K. S. *J. Chem. Phys.* **1995**, *102*, 310.
- Bentwood, R. M.; Barnes, A. T.; Orville-Tomas, W. J. *J. Mol. Spectrosc.* **1980**, *84*, 391.
- Del Bene, J. E.; Pople, J. A. *J. Chem. Phys.* **1970**, *52*, 4858.
- Viant, M. R.; Cruzan, J. D.; Lucas, M. G.; Brown, M. G.; Liu, K.; Saykally, R. J. *J. Phys. Chem. A* **1997**, *101*, 9032.
- David, J. W. *J. Am. Chem. Soc.* **1993**, *115*, 11180.
- Xantheas, S. S.; Dunning, J. T. H. *J. Chem. Phys.* **1993**, *98*, 8037.
- Fowler, J. E.; Schaefer, H. F., III. *J. Am. Chem. Soc.* **1995**, *117*, 446.
- Hodges, M. P.; Stone, A. J.; Xantheas, S. S. *J. Phys. Chem. A* **1997**, *101*, 9163.
- Nielsen, I. M. B.; Seidl, E. T.; Janssen, C. L. *J. Chem. Phys.* **1999**, *110*, 9435.
- Liedl, K. R.; Sekusak, S.; Kroemer, R. T.; Rode, B. M. *J. Phys. Chem.* **1997**, *101*, 4707.
- Liu, K.; Loeser, J. G.; Elrod, M. J.; Host, B. C.; Rzepiela, J. A.; Pugliano, N.; Saykally, R. J. *J. Am. Chem. Soc.* **1994**, *116*, 3507.
- Gregory, J. K.; Clary, D. C. *J. Chem. Phys.* **1995**, *102*, 7817.
- Loerting, T.; Liedl, K. R.; Rode, B. M. *J. Chem. Phys.* **1998**, *109*, 2672.
- Smedarchina, Z. *J. Comput. Chem.* **2001**, *22*, 787.
- Saykally, R. J.; Blake, G. A. *Science* **1993**, *259*, 1570.
- Liu, K.; Cruzan, J. D.; Saykally, R. J. *Science* **1996**, *271*, 929.
- Wales, D. J. *J. Am. Chem. Soc.* **1993**, *115*, 11180.
- Kim, Y.; Corchado, J. C.; Villá, J.; Xing, J.; Truhlar, D. G. *J. Chem. Phys.* **2000**, *112*, 2718.
- Albu, T. V.; Corchado, J. C.; Truhlar, D. G. *J. Phys. Chem. A* **2001**, *105*, 8465.
- Lin, H.; Pu, J.; Albu, T. V.; Truhlar, D. G. *J. Phys. Chem. A* **2004**, *108*, 4112.
- Ischtwan, J.; Collins, M. A. *J. Chem. Phys.* **1994**, *100*, 8080.
- Nguyen, K. A.; Rossi, I.; Truhlar, D. G. *J. Chem. Phys.* **1995**, *103*, 5522.
- Albu, T. V.; Corchado, J. C.; Kim, Y.; Villá, J.; Xing, J.; Truhlar, D. G. MC-TINKERATE 8.8. University of Minnesota: Minneapolis, MN, 2002.
- Corchado, J. C.; Chuang, Y.-Y.; Fast, P. L.; Villá, J.; Hu, W.-P.; Liu, Y.-P.; Lynch, G. C.; Nguyen, K. A.; Jackels, C. F.; Melissas, V. S.; Lynch, B. J.; Rossi, I.; Coitino, E. L.; Fernandez-Ramos, A.; Pu, J.; Steckler, R.; Garrett, B. C.; Isaacson, A. D.; Truhlar, D. G. POLYRATE 8.7.2. University of Minnesota: Minneapolis, MN, 2002.
- Albu, T. V.; Corchado, J. C.; Kim, Y.; Villá, J.; Xing, J.; Truhlar, D. G. MC-TINKER 1.0. University of Minnesota: Minneapolis, MN, 2002.



- (58) Corchado, J. C.; Chuang, Y.-Y.; Coitino, E. L.; Truhlar, D. G. GAUSSRATE 9.0. University of Minnesota: Minneapolis, MN, 2002.
- (59) Frisch, M. J.; Trucks, G. W.; Schlegel, H. B.; Scuseria, G. E.; Robb, M. A.; Cheeseman, J. R.; Zakrzewski, V. G.; Montgomery, J. A., Jr.; Stratmann, R. E.; Burant, J. C.; Dapprich, S.; Millam, J. M.; Daniels, A. D.; Kudin, K. N.; Strain, M. C.; Farkas, O.; Tomasi, J.; Barone, V.; Cossi, M.; Cammi, R.; Mennucci, B.; Pomelli, C.; Adamo, C.; Clifford, S.; Ochterski, J.; Petersson, G. A.; Ayala, P. Y.; Cui, Q.; Morokuma, K.; Salvador, P.; Dannenberg, J. J.; Malick, D. K.; Rabuck, A. D.; Raghavachari, K.; Foresman, J. B.; Cioslowski, J.; Ortiz, J. V.; Baboul, A. G.; Stefanov, B. B.; Liu, G.; Liashenko, A.; Piskorz, P.; Komaromi, I.; Gomperts, R.; Martin, R. L.; Fox, D. J.; Keith, T.; Al-Laham, M. A.; Peng, C. Y.; Nanayakkara, A.; Gonzalez, C.; Challacombe, M.; Gill, P. M. W.; Johnson, B. G.; Chen, W.; Wong, M. W.; Andres, J. L.; Head-Gordon, M.; Replogle, E. S.; Pople, J. A. Gaussian98 (Revision A.11). Gaussian, Inc.: Pittsburgh, PA, 2001.
- (60) Lu, D.-h.; Truong, T. N.; Melissas, V. S.; Lynch, G. C.; Liu, Y.-P.; Garrett, B. C.; Steckler, R.; Lassacson, A. D.; Rai, S. N.; Hancock, G. C.; Lauderdale, J. G.; Joseph, T.; Truhlar, D. G. *Comput. Phys. Commun.* **1992**, *71*, 235.
- (61) Liu, Y.-P.; Lynch, G. C.; Truong, T. N.; Lu, D.-h.; Truhlar, D. G.; Garrett, B. C. *J. Am. Chem. Soc.* **1993**, *115*, 2408.
- (62) Truhlar, D. G.; Isaacson, A. D.; Garrett, B. C. *Theory of Chemical Reaction Dynamics*; Baer, M., Ed.; CRC Press: Boca Raton, FL, 1985; Vol. 4, p 65.
- (63) Truong, T. N.; Lu, D.-h.; Lynch, G. C.; Liu, Y.-P.; Melissas, V. S.; Stewart, J. J. P.; Steckler, R.; Garrett, B. C.; Isaacson, A. D.; Gonzalez-Lafont, A.; Rai, S. N.; Hancock, G. C.; Joseph, T.; Truhlar, D. G. *Comput. Phys. Commun.* **1993**, *75*, 143.
- (64) Liu, Y.-P.; Lu, D.-h.; Gonzalez-Lafont, A.; Truhlar, D. G.; Garrett, B. C. *J. Am. Chem. Soc.* **1993**, *115*, 7806.
- (65) Allison, T. C.; Truhlar, D. G. *Modern Methods for Multidimensional Dynamics Computations in Chemistry*; Thompson, D. L., Ed.; World Scientific: Singapore, 1998; p 618.
- (66) Fast, P. L.; Corchado, J. C.; Sanchez, M. L.; Truhlar, D. G. *J. Phys. Chem. A* **1999**, *103*, 3139.
- (67) Fast, P. L.; Corchado, J. C.; Sanchez, M. L.; Truhlar, D. G. *J. Phys. Chem. A* **1999**, *103*, 5129.
- (68) Fast, P. L.; Truhlar, D. G. *J. Phys. Chem. A* **2000**, *104*, 6111.
- (69) Kim, Y. *J. Am. Chem. Soc.* **1996**, *118*, 1522.
- (70) Kim, Y. *J. Phys. Chem. A* **1998**, *102*, 3025.
- (71) Kim, Y.; Hwang, H. J. *J. Am. Chem. Soc.* **1999**, *121*, 4669.
- (72) Fernandez-Ramos, A.; Truhlar, D. G. *J. Chem. Phys.* **2001**, *114*, 1491.
- (73) Gonzalez-Lafont, A.; Truong, T. N.; Truhlar, D. G. *J. Phys. Chem.* **1991**, *95*, 4618.
- (74) Hu, W. P.; Liu, Y. P.; Truhlar, D. G. *J. Chem. Phys., Faraday Trans.* **1994**, *90*, 1715.
- (75) Corchado, J. C.; Espinosa-Garcia, J.; Hu, W.-P.; Rossi, I.; Truhlar, D. G. *J. Phys. Chem.* **1995**, *99*, 687.
- (76) Smedarchina, Z.; Siebrand, W.; Zgierski, M. Z.; Zerbetto, F. *J. Chem. Phys.* **1995**, *102*, 7024.
- (77) Siebrand, W.; Smedarchina, Z.; Zgierski, M. Z.; Fernández-Ramos, A. *Int. Rev. Phys. Chem.* **1999**, *18*, 5.